# GREEN SYNTHESIS, CHARACTERIZATION, AND ANTIBACTERIAL ACTIVITY OF METAL NANOPARTICLES AND NANOCOMPOSITES USING LEAVES EXTRACT OF *Prunus persica* L.[**]

**Taj Ur Rahman[*], Sadia Mukhtar, Muhammad Aurang Zeb[*], Wajiha Liaqat**

*Mohi-Ud-Din Islamic University, AJ&K, Pakistan; e-mail: taj_urrehman81@yahoo.co.uk, muhammad_aurangzeb@hotmail.com*

*The ZnO, MgO, NiO, and AlO nanoparticles and Zn-Al and Mg-Ni composite oxides were synthesized by the green method from the Prunus persica leaves extract. The synthesized nanoparticles were characterized through FTIR, XRD, SEM, and TEM. The FTIR study was carried out to find out the presence of various functional groups in nanoparticles. Their size was studied by the XRD method which exposed that the nanoparticles were in the range of 19–29 nm, and the size and morphology were studied by SEM, which was further confirmed by TEM. The synthesized nanoparticles were tested for antibacterial activity. In particular, ZnO showed a good inhibitory effect with 22.31 mm of inhibition against Pseudomonas aeruginosa.*

***Keywords:*** *green synthesis, nanoparticle, nanocomposite, leaves extract of Prunus persica.*

# ЭКОЛОГИЧЕСКИ БЕЗОПАСНЫЙ СИНТЕЗ, ХАРАКТЕРИЗАЦИЯ И АНТИБАКТЕРИАЛЬНАЯ АКТИВНОСТЬ МЕТАЛЛИЧЕСКИХ НАНОЧАСТИЦ И НАНОКОМПОЗИТОВ С ИСПОЛЬЗОВАНИЕМ ЭКСТРАКТА ЛИСТЬЕВ *Prunus persica* L.

**T. U. Rahman[*], S. Mukhtar, M. A. Zeb[*], W. Liaqat**

*УДК 546.07:620.3*

*Исламский университет Мохи-Уд-Дин, AJ&K, Пакистан;*
*e-mail: taj_urrehman81@yahoo.co.uk, muhammad_aurangzeb@hotmail.com*

*(Поступила 3 сентября 2021)*

*Наночастицы ZnO, MgO, NiO, AlO и сложные оксиды Zn-Al и Mg-Ni синтезированы экологически безопасным методом из экстракта листьев Prunus persica и охарактеризованы с помощью ИК-Фурье-спектроскопии, рентгеновской дифракции, сканирующей электронной и просвечивающей электронной микроскопии. Для определения наличия различных функциональных групп в наночастицах проведено ИК-Фурье-спектроскопическое исследование. Размер частиц 19—29 нм определен методом рентгеновской дифракции, морфология изучена с помощью сканирующей электронной микроскопии и дополнительно подтверждена с помощью просвечивающей электронной микроскопии. Синтезированные наночастицы протестированы на антибактериальную активность. В частности, показан хороший ингибирующий эффект ZnO (зона ингибирования 22.31 мм) в отношении P. aeruginosa.*

***Ключевые слова:*** *экологически безопасный синтез, наночастица, нанокомпозит, экстракт листьев Prunus persica.*

**Introduction.** Nanotechnology is amongst the most widely used technologies in translational research. The development of metallic nanoparticles employing biological materials by an eco-friendly approach has attracted significant attention. Nanotechnology deals with particles of a size ranging from 1 to 100 nm as well as their synthesis strategy, and manipulation. This knowledge domain naturally commingles all the fields of natural sciences together with chemistry, physics, biological sciences, engineering, materials sci-

[**]Full text is published in JAS V. 89, No. 4 (http://springer.com/journal/10812) and in electronic version of ZhPS V. 89, No. 4 (http://www.elibrary.ru/title_about.asp?id=7318; sales@elibrary.ru).

ence, and computational sciences for the formulation of nanostructures [1, 2]. The nanostructures have different applications attributable to their new or increased properties [3, 4], depending upon their size, distribution, and morphology. It has applications in various fields including biomedical, catalysis, chemical industries, cosmetics, drug delivery, electronics, environment, energy science, food and feed, health care, mechanics, optics, space industries, nonlinear optical devices, single-electron transistors, and photo-electrochemical applications. The metallic nanoparticles are considered as one of the most promising systems for all the aforementioned functions [5–7].

Green chemistry is an emerging area that fosters the implementation of a set of principles intended to reduce the utilization and generation of chemical hazardous wastes [8]. As a result, green methods reduce the industrial labor impact on the ecosystem. Through their development, scientists are providing possible solutions to costly processes and hazardous materials encountered when using traditional physicochemical synthesis methods [9–12]. The employment of environment-friendly solvents and reagents, reducing high energy consumption methods, using nontoxic biomolecules such as DNA, proteins, enzymes, carbohydrates, as well as plant extracts, allow for the synthesizing of biocompatible metallic NPs by reducing metal ions in aqueous solutions [13, 14]. The peach (*Prunus persica* L.) is a climacteric fruit that originated from the Asian continent, mainly China [15]. It is cultivated in many countries, but preferably in temperate regions, as it requires abundant water [16]. It contains a high quantity of water, sugar, and protein along with vitamins and minerals [17]. It also contains phenolic compounds such as catechins and leucoanthocyanins [17]. The major phenolic compounds identified in peaches are chlorogenic acid, catechins, and epicatechins, with other compounds, including gallic acid, ellagic acid, rutin, isoquercetin (primary flavonols), cyanidin glucosides (anthocyanins), and malvin glycosides [18–21]. The presence of carotenoids such as β-cryptoxanthin, β-carotene, and α-carotene, have been detected in the peach fruit together with zeaxanthin, lycopene, and xanthophyll. Peaches are rich in carbohydrates, group B vitamins, including vitamin C (or L-ascorbic acid) and niacin (vitamin B3). The ripe juicy pulp of the fruit is edible, whereas the peel is discarded. The earlier literature shows that the outer peel of the fruit contains higher amounts of phenolics than the pulp, and anthocyanins and flavanols are primarily detected in the peel [17]. Apart from these, the different peach cultivars are rich in hydroxycinnamates and flavan-3-ols with relatively higher antioxidant activities [17, 22, 23].

Keeping in view the aforementioned importance of *Prunus persica* L. and nanoparticles, the current study was carried out to synthesize ZnO, MgO, NiO, and AlO nanoparticles and Mg-Ni and Zn-Al nanocomposite using green synthesis to evaluate their antibacterial potential against various bacterial strains using the agar well diffusion method.

**Materials and methods.** The *Prunus persica* leaves were collected, shade dried, and crushed in a grinder to obtain a fine powder. About 50 g of the dried leaves was taken in a beaker, dipped in distilled water, and placed in a water bath to boil for 10–20 min. After boiling, the mixture was filtered through Whatman No. 1 filter paper. Then 50 mL of the filtered leaf extract was taken in another beaker, and 30 mL of $MgSO_4$ (0.1 mM) was added to it. The solution was mixed well until precipitates were formed. As the precipitates appeared, the solution was allowed to filter. The same procedure was adopted for the synthesis of NiO, $Al_2O_3$, and ZnO nanoparticles by taking their salts. The nanoparticles formed were washed with distilled water, dried for 2 days, and stored for further analysis. Similarly, the synthesis of Mg-Ni composite oxide nanoparticles was prepared by using the $MgSO_4$ solution with a concentration of 0.1 mM and $NiSO_4$ with a concentration of 0.001 mM using the leaf extract as a reducing agent in the aqueous medium. The constant temperature was maintained in the overall process where the MgO and NiO solutions in different ratios (2:3, 1:3, 1:4, and 1:2 v/v) were stirred constantly, and 30 mL of the leaf extract was added to the solution followed by heating of the water bath to 60°C. The color change indicated the formation of composite oxide nanoparticles. The solution was filtered via Whatman No. 1 filter paper. The same procedure was followed for the synthesis of the Zn-Al nanocomposite. The composite nanoparticles were collected and dried in the oven at 60°C.

The nanoparticles obtained were characterized by the FTIR, XRD, SEM, and TEM techniques. The antibacterial activity of the synthesized nanoparticles and composite oxides was evaluated by the agar well diffusion method [24].

**Results and discussion.** *FTIR analysis of the synthesized nanoparticles and nanocomposite.* Fourier transform infrared spectroscopy (FTIR) is used to find out the chemistry of the green synthesized nanoparticles and nanocomposite (Fig. 1). The FTIR spectra of the ZnO NPs synthesized by the green approach show a peak at 530 $cm^{-1}$ corresponding to the hexagonal ZnO symmetric bending vibration, and another peak at 700 $cm^{-1}$ due to the weak vibration of ZnO NPs. The peak observed at 950 $cm^{-1}$ corresponds to the strong

C=C bending vibration of alkene, and the wide peak at 3300 $cm^{-1}$ is due to the strong OH stretching vibration of carboxylic acid. The band observed at 1200 $cm^{-1}$ reflects the presence of the strong C–O stretching of vinyl ether, while the band at 1150 $cm^{-1}$ indicates the presence of the strong C–O of aliphatic ether. The FTIR spectrum obtained for aluminum oxide nanoparticles reveals absorption bands at 3300, 1700, 1550, 1200, 960, and 518 $cm^{-1}$. The peak observed at 3300 $cm^{-1}$ is due to the strong OH stretching vibration of carboxylic acid, while that at 1700 $cm^{-1}$ corresponds to the strong C=O stretching vibration of the conjugated aldehyde. The peaks at 1550, 1200, and 960 $cm^{-1}$ are due to the strong N–O stretching vibration of a nitro compound, the strong C–O stretching of alkyl aryl ether, and the strong C=C bending of alkene, respectively. The peak at 518 $cm^{-1}$ confirms the presence of aluminum oxide nanoparticles. Similarly, the peak around 3300 $cm^{-1}$ on the FT-IR spectrum corresponds to the strong broad O–H stretching vibration of carboxylic acid, and at 1650 $cm^{-1}$ is due to the strong C=O stretching vibration of δ-lactam. The peak observed at 1500 $cm^{-1}$ indicates the presence of the strong N–O stretching of a nitro compound, whereas the peak observed at 1000 $cm^{-1}$ indicates the presence of the strong C=C bending vibration of alkene, while that at 850 $cm^{-1}$ shows the C=C bending of alkene. The band at 790 $cm^{-1}$ is associated with the medium C=C bending of alkene and that at 630 $cm^{-1}$ is assigned to the Ni–O–H stretching bond. The preceding information confirms the formation of pure NiO nanoparticles. In addition, the data obtained from the FTIR results of MgO reveals a band at 3300 $cm^{-1}$, which indicates the strong broad O–H stretching vibration corresponding to carboxylic acid. The band at 800 $cm^{-1}$ displays the existence of the medium C=C bending of alkene, while the absorption band at 950 $cm^{-1}$ indicates the presence of the strong C=C bending vibration of alkene. Similarly, the absorption bands at 1100 and 1400 $cm^{-1}$ display the medium O–H bending due to phenol. The peak at 1900 $cm^{-1}$ shows the medium C=C=C stretching due to allene, while that at 2000 $cm^{-1}$ indicates the presence of C=C=N stretching due to ketenimine. The absorption band at 2200 $cm^{-1}$ indicates the weak stretching of CΞC which corresponds to the presence of alkyne. The absorption bands observed at 550 $cm^{-1}$ indicate the presence of MgO nanoparticles.

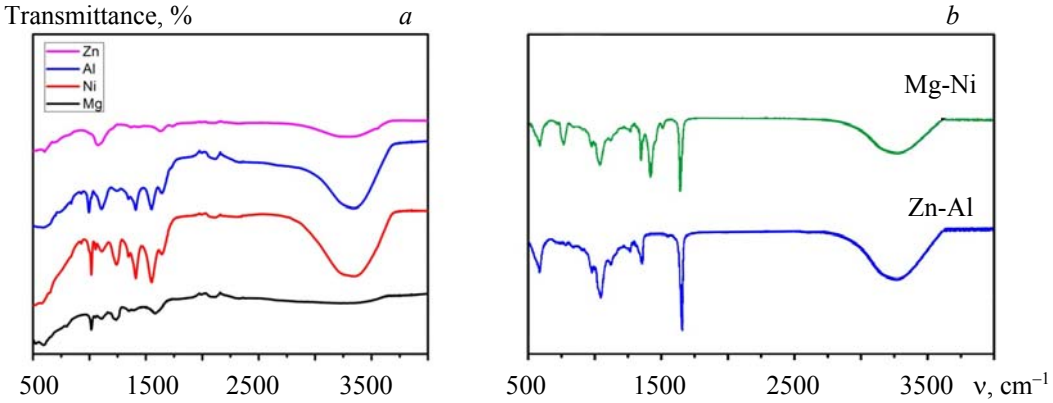


Fig. 1. FTIR spectrum of the synthesized nanoparticles (a) and nanocomposites (b).

In addition, the FTIR spectrum of the nanocomposite (Mg-Ni) absorption peak at 3300 $cm^{-1}$ is due to the strong O–H stretching vibration of carboxylic acid, while the band at 1650 $cm^{-1}$ corresponds to the strong C=O stretching vibration of δ-lactam. The peak at 1500 $cm^{-1}$ is due to the strong N–O stretching of a nitro compound, and that at 1450 $cm^{-1}$ is due to the medium C–H bending vibration of alkane. The peak at 1250 $cm^{-1}$ is due to the strong stretching vibration of the C–O group of aromatic esters, while that at 1095 $cm^{-1}$ is due to the strong C–O stretching vibration of a secondary alcohol. The peak observed at 1040 $cm^{-1}$ corresponds to the strong CO–O–CO stretching vibration of anhydride, while that at 960 $cm^{-1}$ is due to the strong C=C bending vibration of alkene. The peaks observed at 710 and 550 $cm^{-1}$ indicate the presence of Ni and Mg of Mg-Ni nanocomposite. Similarly, the FTIR analysis is frequently used for the characterization of green synthesized nanocomposite oxides of aluminum and zinc. The bands that appeared in the FTIR spectrum are 3300, 1650, 1450, 1434, 1218, 1089, 960, 840, and 550 $cm^{-1}$. The peak that appeared at 3300 $cm^{-1}$ corresponds to the strong O–H stretching vibration of carboxylic acid and that at 1650 $cm^{-1}$ is due to the medium C=C stretching vibration of cyclic alkene. Similarly, the peaks that appeared at 1450 and 1434 $cm^{-1}$ are due to the medium C–H bending of alkanes and the medium O–H bending of carboxylic acid. The band at 1218 and 1089 $cm^{-1}$ is due to the strong C–O stretching vibration of vinyl

ether and the strong C–O stretching of a secondary alcohol. The peaks observed at 960 and 840 $cm^{-1}$ are due to the strong C=C of alkene and the medium C=C bending of alkene. The peak observed at 550 $cm^{-1}$ represents the Al-O stretching mode. The absorption band around 500 $cm^{-1}$ corresponds to the stretching mode of the Zn-O of Zn-Al nanocomposite.

*XRD analysis of the synthesized nanoparticles and nanocomposite.* The XRD technique was used to determine the size and structure of the synthesized nanoparticles and nanocomposite (Fig. 2). The size of synthesized NPs was obtained by Debye–Scherrer's formula:

$$D = K\lambda/(\beta\cos\theta),$$

where $D$ is the crystal size; $\lambda$ is the wavelength of the X-ray radiation ($\lambda$ = 0.15406 nm) for Cu$K_\alpha$; $K$ is usually taken as 0.9, and $\beta$ is the line width at a half-maximum height.

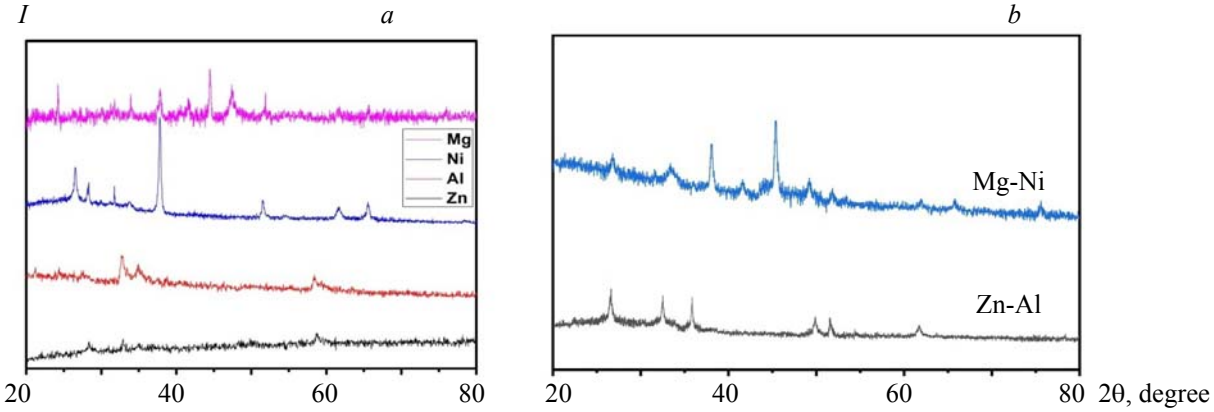


Fig. 2. XRD spectrum of the synthesized nanoparticles (a) and nanocomposites (b).

The diffractogram of the XRD of ZnO showed peaks at 28, 33, 50, 58° suggesting the hexagonal wurtzite structure, the crystal size calculated for ZnO NPs using Scherrer's formula was about 24 nm. The XRD profile of MgO NPs showed peaks at 25, 35, 38, and 58°. The XRD spectrum suggests that MgO NPs were crystalline, the crystal sizes of MgO NPs calculated using Scherrer's formula were about 19 nm. The XRD peaks that appeared at 26, 27, 32, 38, 52, and 66° showed the face center cubic structure of NiO. The crystalline size of NiO nanoparticles calculated by Scherrer's formula was found to be 29 nm. The X-ray diffraction profile of AlO nanoparticles showed peaks at 24, 38, 45, and 48°, suggesting AlO NPs were crystalline and the size of AlO nanoparticles was calculated to be 27 nm.

Similarly, the XRD technique was also used for the characterization of Mg-Ni and Al-Zn nanocomposite (Fig. 2b). The XRD peaks of Mg-NiO appeared at peaks occurring at 26, 33, 37, and 47° showed the face cubic structure and the size of the nanoparticles to be 18 nm. Furthermore, the XRD peaks of Zn-Al nanocomposite at 27, 33, 37, and 50° showed that both the face cubic structure and its size were calculated at 22 nm. The list of peaks and their respective positions (2θ) for the synthesized NPs and nanocomposites as obtained from the X-Ray diffractometer are shown in Table 1.

TABLE 1. List of Peaks and their Respective Positions (2θ) for the Synthesized Nanoparticles and Nanocomposites as Obtained from the X-Ray Diffractometer

| 2θ, degree | FWHM | Particle's size, nm | 2θ, degree | FWHM | Particle's size, nm |
|---|---|---|---|---|---|
| ZnO nanoparticles | | | AlO nanoparticles | | |
| 28 | 0.71 | 12 | 24 | 0.28 | 30 |
| 33 | 0.32 | 27 | 38 | 0.37 | 24 |
| 50 | 0.24 | 38 | 45 | 0.23 | 39 |
| 58 | 0.56 | 17 | 48 | 0.64 | 14 |
| MgO nanoparticles | | | Zn-Al composite | | |
| 25 | 0.31 | 27 | 27 | 0.31 | 28 |
| 35 | 0.62 | 14 | 33 | 0.42 | 21 |

*Continue Table 1*

| 2θ, degree | FWHM | Particle's size, nm | 2θ, degree | FWHM | Particle's size, nm |
|---|---|---|---|---|---|
| NiO nanoparticles | | | Mg-Ni composite | | |
| 38 | 0.74 | 12 | 37 | 0.37 | 24 |
| 58 | 0.46 | 21 | 50 | 0.52 | 17 |
| 27 | 0.41 | 21 | 26 | 0.57 | 15 |
| 38 | 0.32 | 27 | 33 | 0.63 | 14 |
| 52 | 0.24 | 38 | 37 | 0.43 | 20 |
| 66 | 0.35 | 28 | 47 | 0.38 | 24 |

N o t e. X-ray wavelength is 0.15416 nm, Scherrer constant $K = 0.9$.

*SEM results of the synthesized nanoparticles and composite oxide.* The morphological features of the prepared nanoparticles and composite oxides were studied using SEM, as presented in (Fig. 3). The SEM results showed that ZnO nanoparticles were sphere-shaped and their size range was 37 nm (Fig. 3a), likewise, the SEM images of the synthesized AlO nanoparticles reveal that the particles are crystalline with the size range of 40 nm (Fig. 3b). Similarly, from the scanning electron microscopy (SEM) results, it was observed that the size of NiO nanoparticles was in the range of 43 nm and represented the crystalline shape of particles (Fig. 3c). The SEM results of the synthesized MgO nanoparticles reveal that the particles are crystalline in shape and their size range is 28 nm (Fig. 3d). Similarly, the SEM results perceive that the nanocomposites of Zn-Al have a spherical shape and their sizes lie in the range of 26 nm (Fig. 3e); furthermore, the nanocomposites of Mg-Ni have a crystal shape and sizes are ~30 nm (Fig. 3f).

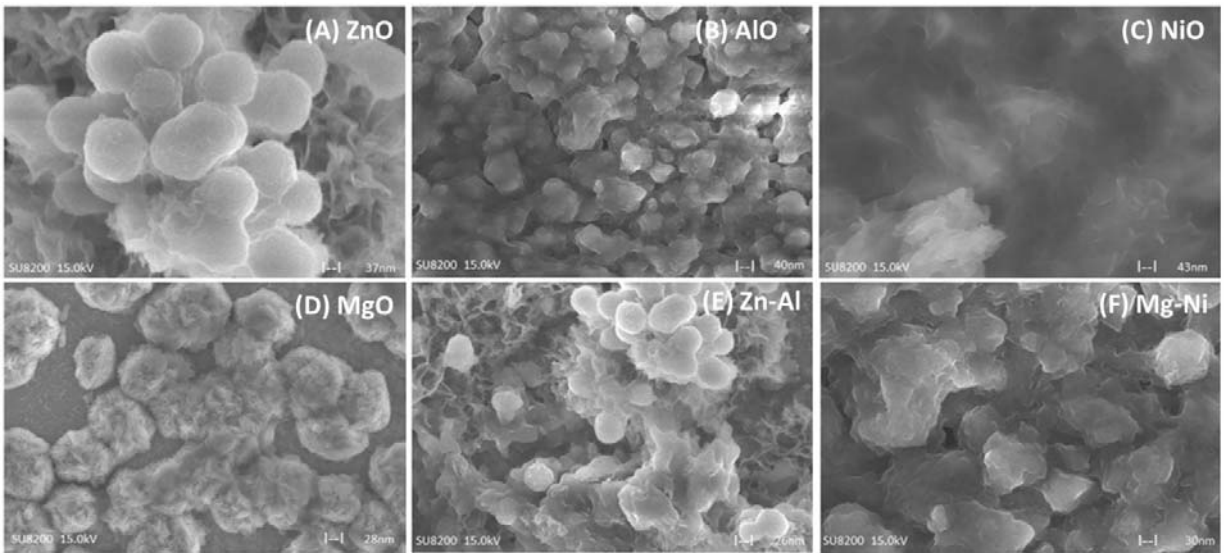


Fig. 3. SEM results of the synthesized nanoparticles and nanocomposite.

*TEM results of the synthesized nanoparticles and a composite oxide.* The size of the synthesized nanoparticles and nanocomposites was characterized using transmission electron microscopy (TEM). As is already known, TEM is an extremely useful technique to obtain direct information concerning the particle size distribution, the mean particle size, and the shape of nanoparticles. Transmission electron microscopy has a 1000 times higher resolution than scanning electron microscopy does [25]. In this study, it was decided to use both methods to measure the size of nanoparticles. The analysis was carried out and the images at different magnifications 19 and 36 nm are shown in (Fig. 4). The TEM image of ZnO in Fig. 4a clearly shows that the nanoparticles are mostly spherical with a size of 25 nm, and the TEM results of AlO nanoparticles depicted in Fig. 4b confirm their crystalline nature and a size of 27 nm. From the TEM analysis, it is observed that the size of NiO nanoparticles is 36 nm with a crystalline shape (Fig. 4c). Similarly, the TEM result of the synthesized MgO nanoparticles (Fig. 4d) confirms the crystal shape with a size of 22 nm. In addition, it is observed that the size of the Zn-Al nanocomposite is 19 nm with a spherical shape (Fig. 4e). Furthermore, the size of Mg-Ni is observed to be 23 nm with a crystal shape (Fig. 4f).

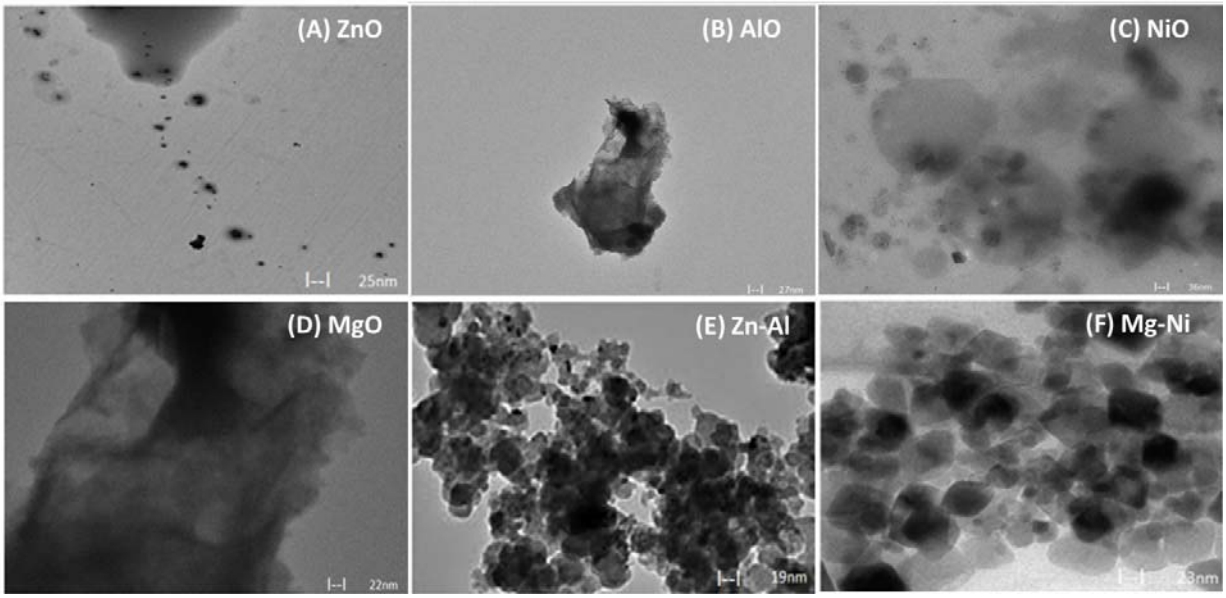


Fig. 4. TEM results of the synthesized nanoparticles and nanocomposites.

*Antibacterial activity.* The green synthesized ZnO, MgO, NiO, and AlO nanoparticles and Mg-Ni and Zn-Al composite oxides were tested for their antibacterial potential against various bacterial strains including *Bacillus cereus*, *Escherichia coli*, *Klebsiella pneumoniae*, *Pseudomonas aeruginosa*, and *Staphylococcus aureus* using the agar well diffusion method. The results obtained (Fig. 5) revealed that NiO and Mg-Ni nanoparticles showed inhibition of 19.21 and 19.20 mm against *B. cerus*, MgO and AlO exhibit inhibition of 19.84 and 19.83 mm against *E.coli*, Zn-Al showed inhibition of 19.20 mm against *K. pneumoniae*, similarly, ZnO showed inhibition of 22.31 mm against Pseudomonas *aeruginosa,* while Mg-Ni composite showed 19.50 mm inhibition against *S. aureus*. Ampicillin was used as a positive control, and DMSO was used as a negative control.

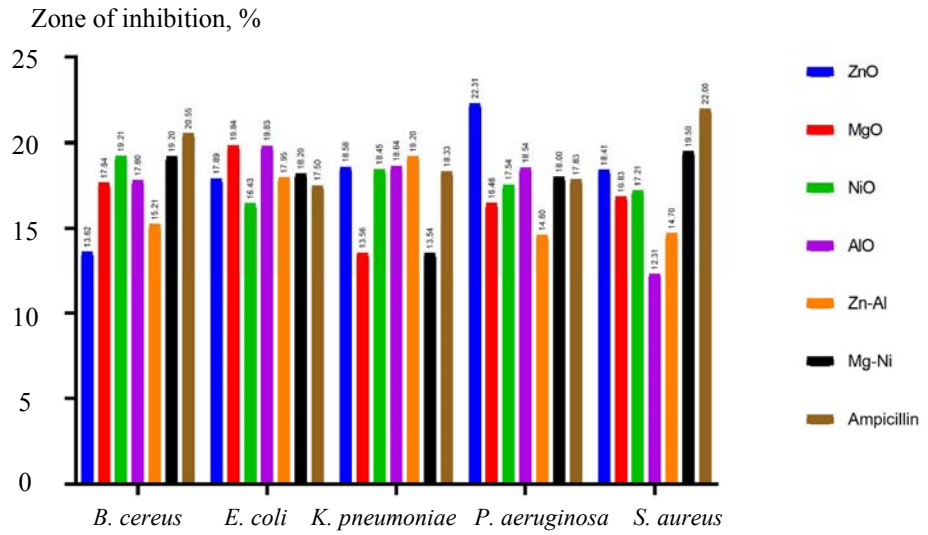


Fig. 5. Antibacterial activity of the synthesized nanoparticles and nanocomposites.

**Conclusions.** The ZnO, MgO, NiO, and AlO nanoparticles and Zn-Al and Mg-Ni nanocomposite were effectively synthesized through the green synthesis method using the *Prunus persica* leave extract, which showed interesting properties. Different techniques were used for the characterization of the synthesized nanoparticles, such as FTIR, XRD, SEM, and TEM, confirming the chemistry, size, and morphology of the synthesized nanoparticles and nanocomposites. The antibacterial activity of the nanoparticles was tested

against *Bacillus cereus*, *Escherichia coli*, *Klebsiella pneumoniae*, *Pseudomonas aeruginosa*, and *Staphylococcus aureus* using the agar well diffusion method. The best results were obtained for ZnO with 22.31 mm of inhibition against *Pseudomonas aeruginosa.* The results confirmed that the synthesized nanoparticles revealed interesting characteristics for various potential applications in the future. Moreover, the results of the current study need to be validated by testing these materials for their in vivo application.

**Acknowledgements.** The authors are grateful to Mohi-Ud-Din Islamic University, Nerian Sharif, Azad Jammu, and Kashmir for providing research facilities.

## REFERENCES

1. W. Shenton, T. Douglas, M. Young, G. Stubbs, S. Mann, *Adv. Mater*., **11**, 230–256 (1999).
2. N. V. Medvedeva, O. M. Ipatova, Y. D. Ivanov, A. I. Drozhzhin, A. I. Archakov, *Biochem. (Moscow), Suppl. B: Biomed. Chem.*, **1**, 114–124 (2007), doi: 10.1134/S1990750807020023.
3. S. Tang, C. Mao, Y. Liu, D. Q. Kelly, S. K. Banerjee, *IEEE Trans. Electron. Devices*, **54**, 433–438 (2007), doi: 10.1109/TED.2006.890234.
4. K. Thakkar, S. Mhatre, R. Parikh, *Nanotechnol. Biol. Med*., **6**, 257–262 (2009), doi: 10.1016/j.nano.2009.07.002.
5. L. Wang, X. Chen, J. Zhan, Y. Chai, C. Yang, L. Xu, et al., *J. Phys. Chem. B*, **109**, 3189–3194 (2005), doi: 10.1021/jp0449152.
6. H. You, S. Yang, B. Ding, H. Yang, *Chem. Soc. Rev.*, **42**, 2880–2904 (2013), doi: 10.1039/C2CS35319A.
7. P. Singh, Y.-J. Kim, D. Zhang, D.-C. Yang, *Trends Biotechnol.*, **34**, 588–599 (2016), doi: 10.1016/j.tibtech.2016.02.006.
8. R. S. Varma, *Curr. Opin. Chem. Eng*., **1**, 123–128 (2012).
9. L. F. B. Nogueira, É. J. Guidelli, S. M. Jafari, A. P. Ramos, In: *Handbook of Food Nanotechnology*, Ed. S. M. Jafari, Academic Press, Cambridge, MA, USA, 257–278 (2020), ISBN 978-0-12-815866-1.
10. M. Hekmati, S. Hasanirad, A. Khaledi, D. Esmaeili, *Gene Rep*., **19**, 100589 (2020).
11. M. Khalaj, M. Kamali, M. E. V. Costa, I. Capela, *J. Clean. Prod*., **267**, 122036 (2020).
12. M. Yadi, E. Mostafavi, B. Saleh, et al., *Cells Nanomed. Biotechnol*., **46**, S336–S343 (2018).
13. D. Hou, D. O'Connor, In *Sustainable Remediation of Contaminated Soil and Groundwater*, Ed. D. Hou, Butterworth-Heinemann, Waltham, MA, USA, 1–17 (2020) ISBN 978-0-12-817982-6.
14. M. Fasciotti, *Sustain. Chem. Pharm*., **6**, 82–89 (2017).
15. S. Pizato, W. R. Cortez-Vega, J. T. A. de Souza, C. Prentice-Hernández, C. D. Borges, *J. Food Safety*, **33**, No. 1, 30–39 (2013).
16. R. Scorza, *Peach and Apricot. Processing Fruits: Science and Technology*, CRC Press, New York, 481–483 (2005).
17. X. Zhao, W. Zhang, X. Yin, et al., *Int. J. Mol. Sci.*, **16**, No. 3, 5762–5778 (2015).
18. G. W. Cheng, C. H. Crisosto, *J. Am. Soc. Horticult. Sci.*, **120**, No. 5, 835–838 (1995).
19. S. Chang, C. Tan, E. N. Frankel, D. M. Barrett, *J. Agric. Food Chem.*, **48**, No. 2, 147–151 (2000).
20. B. A. Cevallos-Casals, D. Byrne, W. R. Okie, L. Cisneros-Zevallos, *Food Chem.*, **96**, No. 2, 273–280 (2006).
21. R. Infante, L. Contador, P. Rubio, D. Aros, Á. Peña-Neira, *Chil. J. Agric. Res.*, **71**, No. 3, 445 (2011).
22. E. Bakir, N. Türker, Ö. İstanbullu, *Gıda*, **32**, No. 1, 15–23 (2007).
23. G. Montevecchi, G. V. Simone, M. G. Mellano, F. Masino, A. Antonelli, *Fruits*, **68**, No. 3, 195–207 (2013).
24. Taj Ur Rahman, Hammad Khan, Wajiha Liaqat, Muhammad Aurang Zeb, *Microscopy Res. Tech*. (**2021**), doi: 10.1002/jemt.23896.
25. A. S. Eppler, J. Zhu, E. A. Anderson, G. A. Somorjai, *Top Catal*., **13**, 33–41 (2000).